ARTICLES

Theoretical Study of Two-Photon above Threshold Dissociation and Related Processes in Na_2^+ and Li_2^+

Sylvie Magnier

Laboratoire de Physique Moléculaire et des Collisions, Institut de Physique, 1 boulevard Arago, Technopôle 2000, F-57078 Metz Cedex 3, France

Maurizio Persico*

Dipartimento di Chimica e Chimica Industriale, Università di Pisa, via Risorgimento 35, I-56126 Pisa, Italy

Naseem Rahman

Dipartimento di Scienze Chimiche, Università di Trieste, via Giorgieri 1, I-34127 Trieste, Italy

Received: May 26, 1999; In Final Form: September 17, 1999

We present wavepacket dynamics simulations of above threshold dissociation (ATD) in Na_2^+ and Li_2^+. We consider resonant two-photon processes in which both the intermediate and the final state belong to the dissociative continuum. We show that in both molecular ions ATD experiments can be planned with moderately high laser intensities. If a vibrational initial state other than $v = 0$ is selected and/or a two-color excitation is envisaged, a wider range of processes can be observed, such as interference phenomena and Rabi oscillations between continuum states.

1. Above Threshold Dissociation Processes and Wave-Packet Dynamics

In previous papers[1,2] we have proposed a "minimal scenario" for above threshold dissociation (ATD) experiments in the molecular ion Na_2^+. ATD was proposed long ago[3] as the analogous of above threshold ionization in the framework of the vibrational continuum states of molecules. The idea is to induce dissociation by absorption of a number of photons larger than the minimum required to reach the dissociation limit, therefore causing one or more free−free transitions. Experiments[4] and calculations[5−7] demonstrating the ATD phenomenon were performed on molecular ions (H_2^+ and Na_2^+), a choice which minimizes the competing process of (further) ionization. When the field frequency is such that no intermediate resonant states are present, as in previous work by other authors,[4−6] rather strong laser pulses are needed: for instance, experiments[4] on H_2^+ employed 100 ps laser pulses with $\lambda = 532$ nm and intensities over 50 TW/cm^2; simulations by Jolicard and Atabek[6] with $\lambda = 330$ nm and ultrashort pulses (20 fs) yielded significant photodissociation probabilities (>1%) only with peak powers larger than 100 TW/cm^2, i.e., total energies of 2 J/cm^2.

In our minimal scenario we envisage a two-photon process with a dissociative resonant intermediate state. This means that the first photon hits a strong bound-free absorption band and can cause dissociation by itself; however, before the molecule falls apart, a second photon may be absorbed, so that dissociation will take place in another repulsive potential energy curve. The one- and two-photon processes can be experimentally distinguished because the products (atoms and atomic ions) differ as to electronic state and translational kinetic energy. Calculations on Na_2^+, limited to the $^2\Sigma_{g,u}^+$ manifold, were performed for two selected laser frequencies by Machholm and Suzor-Weiner:[7] they showed that ATD can be obtained with much weaker fields (100 GW/cm^2 peak power, 3×10^{-3} J/cm^2 pulse energy). In computing Na_2^+ photodissociation spectra,[1,2] we applied still lower intensities (1 GW/cm^2 peak power, 10^{-4} J/cm^2 pulse energy). In these conditions, the phenomenon of bond-softening[4−6] and the multiphoton transitions not enhanced by the presence of resonant intermediate states are not important: we shall therefore discuss our results in terms of sequential one-photon transitions between unperturbed molecular states.

Na_2^+ features two excited states, $1^2\Sigma_{g,u}^+$ and $1^2\Pi_g$, with vertical excitation energies in the approximate ratio $^1/_2$, so that the transitions $1^2\Sigma_g^+(v = 0) \rightarrow 1^2\Sigma_u^+$ and $1^2\Sigma_u^+ \rightarrow 1^2\Pi_g$ can take place with the same photon energy, being favored by large Franck−Condon factors. However, one cannot expect to find the same favorable conditions in all systems: Li_2^+ is one example, as shown in section 3.B of this paper. Two ways out of this difficulty can be envisaged: either to start with a higher vibrational level or to use two radiation pulses with different frequencies. In this work, therefore, we have generalized our preliminary results on Na_2^+, by studying the effect of the initial vibrational state (section 3) and by proposing two-color experiments (section 4); moreover, we have extended our investigation to Li_2^+. Doing so, we have come by some new processes, related

* To whom correspondence should be addressed. E-mail: mau @hermes. dcci. unipi. it.

10.1021/jp9917291 CCC: $18.00
Published on Web 11/24/1999

to ATD, such as Rabi oscillations between continuum states[8] and radiation−molecular interference.

2. Model and Method

In order to evaluate quantitatively the photodissociation probabilities, we run simulations of the process, with a quantum mechanical, time-dependent description of the molecular system interacting with a classical radiation field. The most important approximations introduced in this model are the Born−Oppenheimer separation and the neglect of molecular rotation. The former is justified by the absence of avoided crossings in the homonuclear systems considered in previous papers and in the present one. Ignoring rotation in a first approximation amounts to overestimating the effect of a given radiation pulse,[1] as if the intensity would be multiplied by a factor depending on the initial rotational quantum numbers and on the type of transitions involved (parallel versus perpendicular).

The Hamiltonian contains a molecular term, $\hat{H}_0$, and a dipolar coupling:

$$\hat{H} = \hat{H}_0 - \epsilon\mu \tag{1}$$

Here μ is the molecular dipole and the electric field ϵ represents one or two linearly polarized radiation pulses, each with an amplitude A_k, a carrier frequency Ω_k, and a finite length τ_k (fwhm of the intensity) centered at time t_k. Within the duration of the kth radiation pulse ($|t - t_k| < \tau_k$), the electric field is:

$$\epsilon(t) = A_k \cos(\Omega_k t) \cos\left(\frac{\pi(t - t_k)}{2\tau_k}\right) \tag{2}$$

The peak intensity for such a radiation pulse is $I_{max} = cA_k^2/8\pi$, while the integrated intensity or total pulse area is $I_{tot} = cA_k^2\tau_k/8\pi = I_{max}\tau_k$. Our standard pulse length is 10 fs, with integrated intensities of 0.005 au $= 7.8 \times 10^{-4}$ J/cm^2, i.e., peak intensities of 78 GW/cm^2.

The pulse length of 10 fs corresponds to a bandwidth $\Delta\nu$ of about 1200 cm^{-1} (hwhm), so details of the photodissociation spectra requiring higher resolution will be washed out. In particular, the bound-bound $1^2\Sigma_g^+ \rightarrow 1^2\Pi_u$ subbands are all convoluted together and they connect smoothly with the bound-free part of the spectrum, as illustrated elsewhere in more detail.[13] In our previous work[1] we have shown that longer pulses (about 100 fs) yield higher cross sections for a particular two-photon excitation process in Na_2^+. This is because narrower bandwidths allow us to concentrate more radiating power in the resonance region of the two-photon spectrum. However, still longer pulses result in a loss of efficiency, because molecular dissociation competes with the absorption of the second photon. Lighter atomic masses (Li_2^+ versus Na_2^+) will shift the balance towards shorter pulses. Another feature, namely, the Rabi oscillations described in section 4.C, requires short pulses to be observed. We have adopted the 10 fs pulse length because it is a viable compromise for all kinds of processes and it minimizes the computational burden.

The finite bandwidth is also the fundamental source of uncertainty in the kinetic energy spectrum of the ejected atoms or ions, which can be measured in order to discriminate between one- and two-photon dissociation. For a homonuclear diatomic, both products will have approximately the same final velocity. Each of them will be endowed with a kinetic energy E_K, depending on the n-photon nature of the transition:

$$E_K = \frac{nh\upsilon + E_v - D_e - E^*}{2} \tag{3}$$

Here $nh\upsilon$ is the energy of the n absorbed photons (it should be replaced by $n_1h\upsilon_1 + n_2h\upsilon_2$ in two-color experiments), E_v is the initial vibrational energy, D_e is the ground state dissociation energy of the molecular ion, and E^* is the electronic energy of the neutral atom (vanishing for ground state products). The upper bound to the width ΔE_K of the kinetic energy peaks is then $nh\Delta\upsilon/2$, inversely proportional to the pulse length and of the order of 0.1 eV for 10 fs pulses. Narrower peaks may be obtained, compatibly with experimental resolution, depending on the shape of the molecular absorption band, which in turn is determined by the Franck−Condon factors ("reflection principle", see ref 9). In the limit of very short pulses, the energy spread is proportional to the width ΔR of the initial vibrational state and to the slope U′ of the final potential energy curve: starting with $\upsilon = 0$, we have $\Delta E_K = U'\sqrt{\hbar/\omega_0 M}$, where ω_0 is the vibrational frequency in the ground state and M the reduced mass: For Na_2^+ this is in the range 0.1−0.2 eV and for Li_2^+ 0.15−0.5 eV, therefore the width of the peaks in the kinetic energy spectrum will be normally determined by the pulse length τ. A computed spectrum is reported in our previous work (τ = 100 fs, $\Delta E_K \simeq 0.01$ eV).

Our simulations of the photodissociation processes rely on the direct integration of the time-dependent Schrödinger equation (TDSE). The time-dependent wave function is written as

$$|\Psi(R, t)\rangle = \sum_i \chi_i(R, t)|\psi_i(R)\rangle \tag{4}$$

where $\psi_i(R)$ is an adiabatic electronic wave function and $\chi_i(R, t)$ the associated wave packet. The probability of being in a given electronic state is $P_i(t) = \int_0^\infty |\chi_i(R, t)|^2\, dR$. In the absence of radiationless transitions, after the end of the radiation pulse(s), P_i becomes independent of time and gives the probability of photodissociation to the atomic products correlated with the molecular state ψ_i. We integrate the TDSE by the split-operator FFT method, whereby the wave packets χ_i are represented on a space grid and are propagated stepwise in time.[10] A grid of 256 point is used, in the intervals 4−18 bohr for Na_2^+ and 3−18 bohr for Li_2^+. The time step is 0.025 fs in both cases. These values have been found to ensure convergence of the computed probabilities. Notice that the absorbed photons are converted mainly into electronic energy, and only partially into nuclear kinetic energy, during the downhill wave packet motion. Moreover, limiting ourselves to rather short times (typically 40 fs), we never reach the asymptotic region, i.e., the final and largest kinetic energies. As the latter, in turn, do not exceed 1.7 eV (see Table 1), a rather large grid step ($\Delta R \simeq$ 0.05 bohr) can be safely used. The short time−short distance limitation also eliminates the problem connected with divergent dipole matrix elements between asymptotically degenerate gerade/ungerade pairs of states.

Within the adiabatic expansion (eq 4), the Hamiltonian (eq 1) is completely specified by the potential energy curves (see Figures 1 and 2) and by the dipole matrix elements as functions of the internuclear distance R. These ingredients have been computed with high accuracy by a model potential method.[11,12]

3. One-Color Experiments

3.A. Excitation of Na_2^+ ($1^2\Sigma_g^+$, $\upsilon = 0$). All the Na_2^+ calculations take into account the nine states shown in Figure 1. Two excited states of Na_2^+ can be populated by one-photon

TABLE 1: One- and Two-Photon Dissociation Processes: Final Molecular and Atomic States and Translational Kinetic Energies of the Product Atoms and Ions

			one-photon			two-photon		
	initial vibrational state	optimal frequency[a] (cm^{-1})	final molecular state	final atomic state[b]	kinetic energy (eV)	final molecular state	final atomic state	kinetic energy (eV)
Na_2^+	0	15500	$1^2\Sigma_u^+$	3s	0.47	$2^2\Sigma_g^+$	3p	0.38
	0	18900	$1^2\Sigma_u^+$	3s	0.68	$1^2\Pi_g$	3p	0.81
	0	21200	$1^2\Sigma_u^+$	3s	0.82	$3^2\Sigma_g^+$	4s	0.52
	0	22000	$1^2\Pi_u$			$1^2\Delta_g$	3d	0.52
	13	12400	$1^2\Sigma_u^+$	3s	0.37	$2^2\Sigma_g^+$	3p	0.09
	13	18000	$1^2\Sigma_u^+$	3s	0.72	$1^2\Pi_g$	3p	0.79
	13	23300	$1^2\Pi_u$	3p	0.00	$1^2\Delta_g$	3d	0.77
	0	18875/12100	$1^2\Sigma_u^+$	3s	0.68	$2^2\Sigma_g^+$	3p	0.38
	0	18875/23700	$1^2\Sigma_u^+$	3s	0.68	$3^2\Sigma_g^+$	4s	0.60
Li_2^+	0	26000	$1^2\Pi_u$	2p	0.05	$1^2\Delta_g$	3d	0.62
	10	11800	$1^2\Sigma_u^+$	2s	0.25	$2^2\Sigma_g^+$	2p	0.05
	10	14800	$1^2\Sigma_u^+$	2s	0.43	$1^2\Pi_g$	2p	0.43
	10	20500	$1^2\Pi_u$			$3^2\Sigma_g^+$	3s	0.39
	10	21900	$1^2\Pi_u$			$1^2\Delta_g$	3d	0.27
	0	24140/8300	$1^2\Sigma_u^+$	2s	0.86	$2^2\Sigma_g^+$	2p	0.45
	0	24140/14400	$1^2\Sigma_u^+$	2s	0.86	$1^2\Pi_g$	2p	0.83
	0	24140/25500	$1^2\Pi_u$			$3^2\Sigma_g^+$	3s	0.77
	0	24140/27900	$1^2\Pi_u$			$1^2\Delta_g$	3d	0.62

[a] Frequency corresponding to the peak of the two-photon absorption band. When two frequencies are indicated, they refer to first and second pulses in two-color experiments. [b] State of the neutral atom at dissociation. When not indicated, the final molecular state is bound (no direct dissociation).

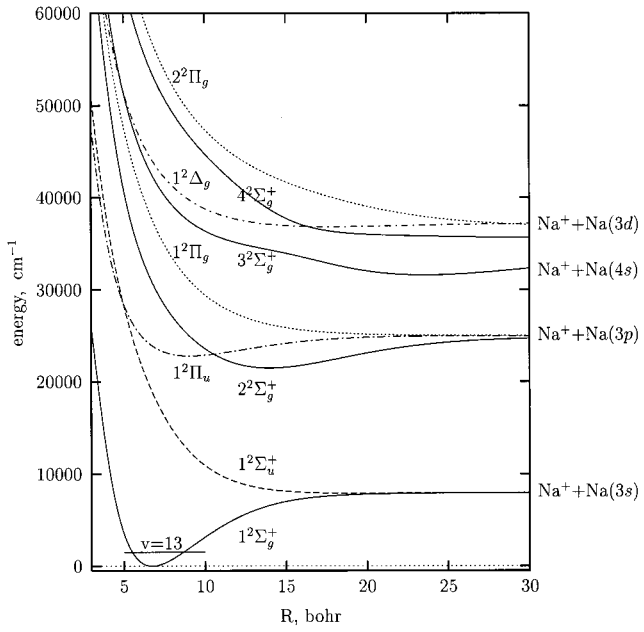

Figure 1. Potential energy curves of Na_2^+.

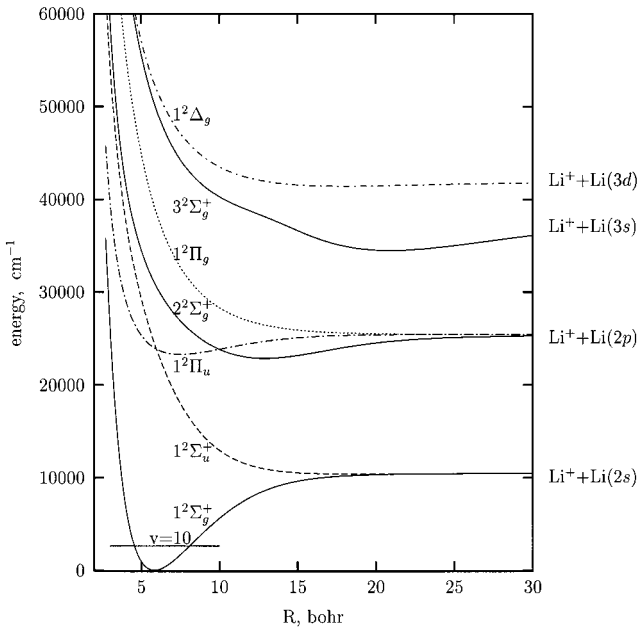

Figure 2. Potential energy curves of Li_2^+.

absorption with frequencies lower than 30000 cm^{-1}: $1^2\Sigma_u^+$ and $1^2\Pi_u$. The former has a completely repulsive potential, correlating to the same dissociation limit as the ground state, i.e., Na^++Na(3s). The latter accomodates in its potential well 68 bound states, with transition energies between 22766 and 24910 cm^{-1}, starting from $1^2\Sigma_g^+$, $v = 0$. The one-photon transitions to $1^2\Sigma_u^+$ and $1^2\Pi_u$ account for the two largest peaks in the spectrum of Figure 3. Only the higher frequency wing of the $1^2\Pi_u$ peak is related to dissociating states, therefore a two-photon excitation having $1^2\Pi_u$ as the intermediate state cannot be qualified as ATD (this is the case of the weak $1^2\Delta_g$ absorption). It should be noted that with a pulse bandwidth of 1000 cm^{-1} the limit between the bound-bound and bound-free parts of the spectrum is rather flou (see also ref 13).

The main two-photon ATD process taking place when starting with $v = 0$ ends up in the $1^2\Pi_g$ state and the atomic product is Na(3p): the corresponding absorption band (see Figure 3) peaks at about the same frequency as the one-photon transition to $1^2\Sigma_u^+$, due to the fortuitous equidistance of the potential energy curves. Two more features of the absorption spectrum lie within the left and right wings of the $1^2\Sigma_u^+$ band and represent weaker two-photon transitions, leading respectively to the $2^2\Sigma_g^+$ and $3^2\Sigma_g^+$ states. In Table 1 we list the relevant parameters of all the ATD processes we have computed. It can be seen that the one- and two-photon peaks in the kinetic energy spectrum which can be obtained at the optimal frequency of 18900 cm^{-1} differ by only 0.13 eV.

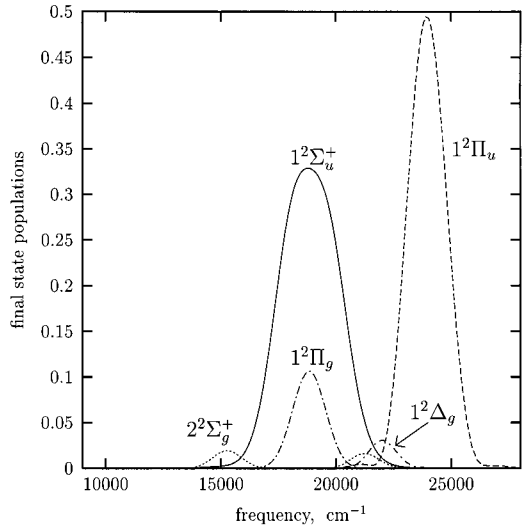

Figure 3. One-color excitation of Na_2^+, $1^2\Sigma_g^+$, $v = 0$. Pulse parameters: $\tau = 10$ fs, $I_{tot} = 0.005$ au, $I_{max} = 7.8 \times 10^{10}$ W/cm^2.

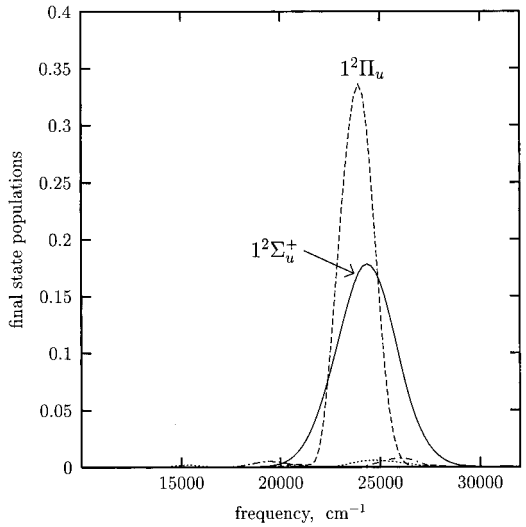

Figure 4. One-color excitation of Li_2^+, $1^2\Sigma_g^+$, $v = 0$. Pulse parameters: $\tau = 10$ fs, $I_{tot} = 0.005$ au, $I_{max} = 7.8 \times 10^{10}$ W/cm^2.

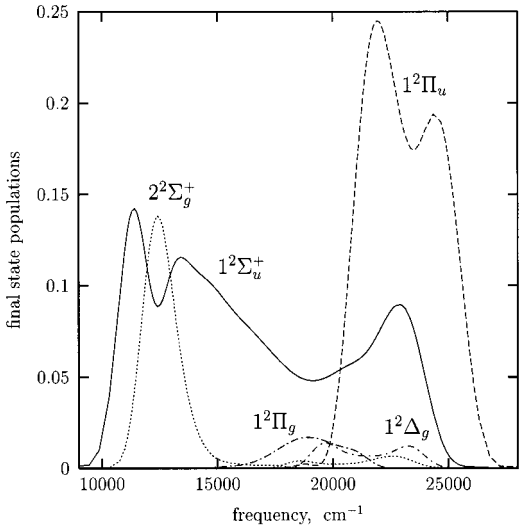

Figure 5. One-color excitation of Na_2^+, $1^2\Sigma_g^+$, $v = 13$. Pulse parameters: $\tau = 10$ fs, $I_{tot} = 0.005$ au, $I_{max} = 7.8 \times 10^{10}$ W/cm^2.

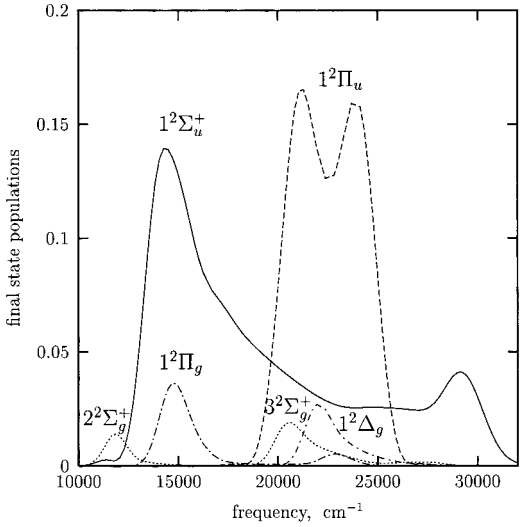

Figure 6. One-color excitation of Li_2^+, $1^2\Sigma_g^+$, $v = 10$. Pulse parameters: $\tau = 10$ fs, $I_{tot} = 0.005$ au, $I_{max} = 7.8 \times 10^{10}$ W/cm^2.

3.B. Excitation of Li_2^+ ($1^2\Sigma_g^+$, $v = 0$). The potential energy curves of Li_2^+ are quite similar to those of Na_2^+ (see Figure 2). However, the vertical excitation energies to the first $^2\Sigma_u^+$ and $^2\Pi_u$ states are much closer in Li_2^+ than in Na_2^+, so the corresponding one-photon absorption bands overlap (see Figure 4). Here too, the $1^2\Pi_u$ potential is attractive, therefore, when starting from $1^2\Sigma_g^+$, $v = 0$, the absorption is mainly due to bound-bound transitions.

The spectral simulations consider all the seven states of Figure 2. For our purposes another important difference with respect to Na_2^+ is that, with frequencies corresponding to the one-photon absorption peaks (24000−25000 cm^{-1}), there are no upper resonant states of gerade symmetry. This is why the two-photon processes are very weak in this case. In Table 1 we list only a two-photon transition to the $1^2\Delta_g$ state which takes place at about 26000 cm^{-1}. This photon energy is barely sufficient to dissociate Li_2^+ in the $1^2\Pi_u$ state, so this process can be qualified as ATD.

3.C. Photodissociation with Initial Excited Vibrational States. The molecular ions can be easily produced in excited vibrational states, by laser ionization of the corresponding neutral molecules.[14] This offers a chance to change the energetic relationships between initial, intermediate, and final states in two-photon excitation. We have explored the spectra which can be obtained with different initial vibrational quantum numbers v. The band shapes and intensities change gradually, also because of the low resolution associated with ultrashort pulses. We have found some interesting features with $v = 13$ for Na_2^+ and $v = 10$ for Li_2^+. The simulation results are shown in Figures 5 and 6. The spectra obtained with initial v's differing by one or two units are similar.

Concerning the one-photon bands, the main difference with respect to the $v = 0$ case is that they are much wider, with two maxima corresponding to the inner and outer turning points of the excited vibrational state. Both for Na_2^+, $v = 13$, and for Li_2^+, $v = 10$, the higher frequency maximum of the $1^2\Pi_u$, absorption band corresponds to bound-free transitions.

In the Na_2^+ two-photon spectrum, the $2^2\Sigma_u^+$ band is greatly enhanced, and the consequent depopulation of the $1^2\Sigma_u^+$ intermediate state makes a distinct dip in the corresponding one-photon band. For these two states the difference in the kinetic energy of the ejected atoms is about 0.3 eV: this time, the 3p atom (two-photon product) is endowed with a smaller E_K than the 3s atom (one-photon); the opposite is obtained with the $1^2\Sigma_u^+ - 1^2\Pi_g$ excitation described in section 3.A. The sizeable

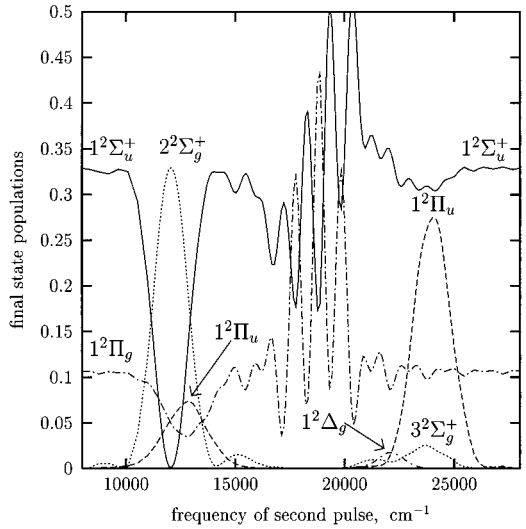

Figure 7. Two-color excitation of Na_2^+, $1^2\Sigma_g^+$, $v = 0$. First pulse: $\tau = 10$ fs, $\Omega_1 = 0.086$ au $= 18875$ cm^{-1}, $I_{tot} = 0.005$ au, $I_{max} = 7.8 \times 10^{10}$ W/cm^2. Second pulse: same as first pulse, with variable Ω_2.

kinetic energy difference and the large intensity of the $2^2\Sigma_g^+$ band probably make this process one of the easiest to detect. The $1^2\Pi_g$ state can be populated by two-photon absorption with either $1^2\Sigma_u^+$ or $1^2\Pi_u$ as the intermediate state. The former is probably more important, at least below 20000 cm^{-1}, in view of the larger population of $1^2\Sigma_u^+$. The process leading to $1^2\Delta_g$, on the contrary, goes necessarily through $1^2\Pi_u$, because of the selection rules. The $1^2\Pi_u$ vibrational states involved are close to the boundary between discrete and continuum spectrum.

In the case of Li_2^+, starting with $v = 10$ brings to existence several two-photon processes that are almost completely suppressed with $v = 0$. In the low-frequency side, the $2^2\Sigma_g^+$ state is populated, with production of very slow 2p atoms (0.05 eV). The $1^2\Pi_g$ absorption at 14800 cm^{-1} yields atoms with the same kinetic energy (0.43 eV) as the corresponding one-photon transition to $1^2\Sigma_u^+$, because the photon energy approximately coincides with that of the transition between the Li(2s) and Li(2p) levels: therefore, in this case it will be difficult to discriminate between atomic and molecular transitions. The $3^2\Sigma_g^+$ and the $1^2\Delta$ bands are almost completely due to resonance with intermediate bound vibrational states of the $1^2\Pi_u$ potential.

4. Two-Color Experiments

4.A. Photodissociation Spectra of Na_2^+ and Li_2^+. The use of two lasers with different frequencies introduces another degree of freedom which can be exploited in order to extend the range of ATD processes. The simulation of two-color experiments implies two successive laser pulses, of lengths τ_1 and τ_2 and carrier frequencies Ω_1 and Ω_2. The delay between the two pulses is $t_2 = \tau_1 + \tau_2$, so that they are contiguous in time but do not overlap. The length and integrated intensity of the first pulse are kept fixed at the standard values of 10 fs and 0.005 au. The frequency Ω_1 corresponds to the peak in the $1^2\Sigma_u^+$ absorption band, i.e., 18875 cm^{-1} for Na_2^+ and 24140 cm^{-1} for Li_2^+.

In a first simulated experiment we change the frequency Ω_2 of the second pulse, with the same length and intensity as in the first pulse. Figure 7 shows the final state populations obtained for Na_2^+. To better distinguish the action of both radiation pulses, in Figure 8 we plot the time-dependent probabilities for $\Omega_2 = 12100$ cm^{-1}. As in one-color experiments,

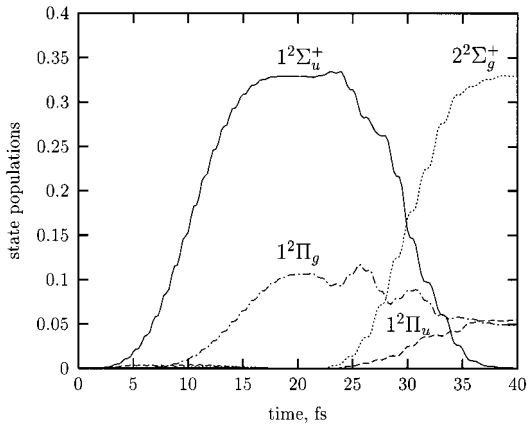

Figure 8. Two-color excitation of Na_2^+, $1^2\Sigma_g^+$, $v = 0$. State populations as functions of time. First pulse: $\tau = 10$ fs, $\Omega_1 = 0.086$ au $= 18875$ cm^{-1}, $I_{tot} = 0.005$ au, $I_{max} = 7.8 \times 10^{10}$ W/cm^2. Second pulse: same as first pulse, with variable Ω_2.

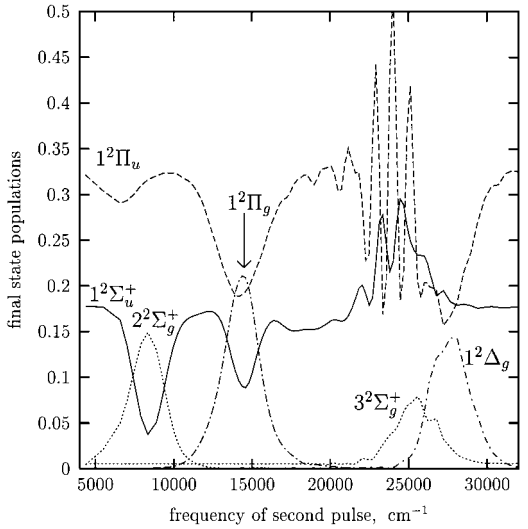

Figure 9. Two-color excitation of Li_2^+, $1^2\Sigma_g^+$, $v = 0$. First pulse: $\tau = 10$ fs, $\Omega_1 = 0.110$ au $= 24140$ cm^{-1}, $I_{tot} = 0.005$ au, $I_{max} = 7.8 \times 10^{10}$ W/cm^2. Second pulse: same as first pulse, with variable Ω_2.

the first pulse populates both $1^2\Sigma_u^+$ (one-photon absorption) and $1^2\Pi_g$ (two-photon). The second pulse brings about a strong $1^2\Sigma_u^+ - 2^2\Sigma_g^+$ transition, with a product kinetic energy difference of 0.3 eV. At slightly higher frequencies, about 13000 cm^{-1}, we have stimulated emission from the $1^2\Pi_g$ continuum to bound levels of $1^2\Pi_u$, a sort of "pump-and-dump" process with a round trip in the dissociative part of the spectrum. The strong $1^2\Pi_u$ band around 24000 cm^{-1} is due to one-photon absorption during the second pulse, and the $3^2\Sigma_g^+$ and $1^2\Delta_g$ states are mainly populated by transitions starting from bound $1^2\Pi_u$ levels.

The Li_2^+ two-color photodissociation spectrum, shown in Figure 9, differs from that of Na_2^+ as the first pulse populates the $1^2\Sigma_u^+$ and $1^2\Pi_u$ states, both by one-photon absorption, instead of $1^2\Sigma_u^+$ and $1^2\Pi_g$. Also here we see an almost complete population switch between $1^2\Sigma_u^+$ and $2^2\Sigma_g^+$, at $\Omega_2 \simeq 8300$ cm^{-1}. The $1^2\Pi_g$ state is populated at the expenses of both $1^2\Sigma_u^+$ (dissociative states) and $1^2\Pi_g$ (bound states), around $\Omega_2 = 14800$ cm^{-1}. The $3^2\Sigma_g^+$ and $1^2\Delta_g$ two- photon absorptions take advantage of the $1^2\Pi_u$ bound levels as intermediate states.

4.B. Interference Phenomena. The rapid oscillations of state probabilities which occur when $\Omega_2 \simeq \Omega_1$, both in the Na_2^+ and in the Li_2^+ case, deserve some discussion. Let us focus first on

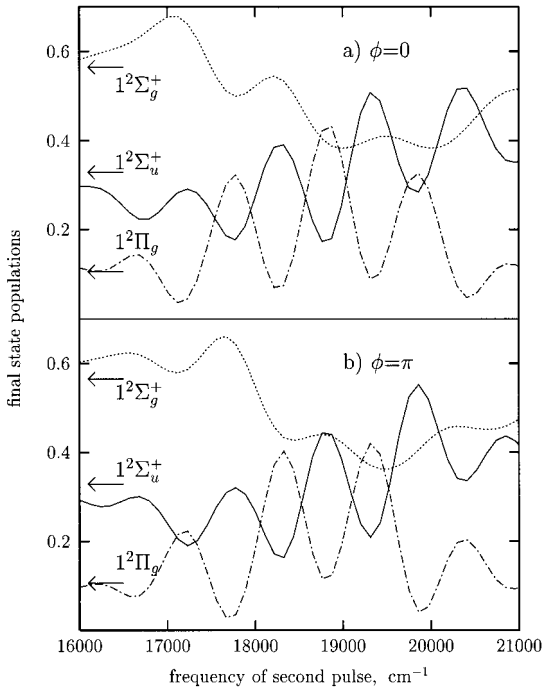

Figure 10. Effect of relative phase of the two laser pulses in the two-color excitation of Na_2^+, $1^2\Sigma_g^+$, $v = 0$. First pulse: $\tau = 10$ fs, $\Omega_1 = 0.086$ au $= 18875$ cm^{-1}, $I_{tot} = 0.005$ au, $I_{max} = 7.8 \times 10^{10}$ W/cm^2. Second pulse: same as first pulse, with variable Ω_2. Arrows indicate populations after the first pulse. ϕ is an additional phase shift between the two pulses: $\phi = 0$ in the upper panel, $\phi = \pi$ in the lower one.

the Na_2^+ spectrum which is shown in more detail in Figure 10a. Such oscillations are a clear fingerprint of interference, but it cannot be direct interference of the two laser pulses, as they do not overlap in time. The first pulse leaves the molecule in a nonstationary state of the form:

$$|\Psi(t)\rangle = \chi_0(R,t)\,|1^2\Sigma_g^+\rangle + \chi_1(R,t)|1^2\Sigma_u^+\rangle + \chi_2(R,t)|1^2\Pi\rangle \quad (5)$$

where χ_0, χ_1, and χ_3 are the wave packets associated with the three electronic states. If the wave packets are well localized, as is the case after a short laser pulse, it is convenient to introduce phase factors taking into account the potential energies E_I computed in the wave packet centroids:

$$\chi_I(R,t) = \bar{\chi}_I(R,t)\mathrm{e}^{-iE_It/\hbar} \quad (6)$$

In general, the time evolution of a wavepacket is the resultant of two contributions: one, $(\partial\bar{\chi}_I/\partial t)_{mol}$, is due to the molecular hamiltonian $\hat{H}_0$ (motion in the electronic potential and nonadiabatic transitions); the other one, $(\partial\bar{\chi}_I/\partial t)_{rad}$, to coupling with the radiation field. In our case, the second laser pulse contributes to the change of shape and norm of a wave packet in the form:

$$\left(\frac{\partial\bar{\chi}_I}{\partial t}\right)_{rad} = \frac{i}{\hbar}\sum_J \epsilon(t)\mu_{IJ}\,\bar{\chi}_J\,\mathrm{e}^{i(E_I-E_J)t/\hbar} \quad (7)$$

When Ω_2 is approximately in resonance with the $I \rightarrow J$ transition, the wave packet $\bar{\chi}_I$ is partially transferred to the electronic state J and vice versa, with opposite phases. Therefore, if $\bar{\chi}_I$ and $\bar{\chi}_J$ overlap significantly, one of the two state populations is increased and the other one decreased. The phase of $(\partial\bar{\chi}_I/\partial t)_{rad}$ depends on the relative phases of $\epsilon(t)$, at the time when its amplitude is largest, and of the molecular factor $\mathrm{e}^{i(E_I-E_J)t/\hbar}$. This is the main parameter which determines whether the interference is constructive or destructive for state I.

The peak intensity of the second pulse is reached with a fixed delay $t_2 = 20$ fs, but a small change in the Ω_2 frequency entails a sizeable change in the phase of the electric field: in fact, $(E_2 - E_1)t_2/\hbar \simeq \Omega_2 t_2 \simeq 20\pi$. The phase changes cause the switching from absorption to stimulated emission which is observed in Figure 10a. The $1^2\Sigma_u^+$ and $1^2\Pi_g$ populations oscillate widely when Ω_2 is approximately in resonance with the relative transition. The $1^2\Sigma_g^+$ state is less affected because, as the wavepackets χ_1 and χ_2 move downhill, their overlap with χ_0 vanishes and the $1^2\Sigma_g^+ - 1^2\Sigma_u^+$ transition goes out of resonance. To confirm this interpretation, we have run simulations where an additional phase shift π is applied to the electric field of the second pulse: as shown in Figure 10b, all the probability oscillations are reversed. In the Li_2^+ case, the population oscillations involve the ground state to a larger extent than with Na_2^+, because here the most intense transitions take place between the two states with attractive potentials, $1^2\Sigma_g^+$ and $1^2\Pi_u$.

Quite clearly, the oscillations will be washed out without a very precise control of the relative phase and time delay of the two laser pulses. This cannot probably be achieved unless the two pulses come from the same laser, therefore with identical frequencies but with a variable delay, thus realizing a sort of "molecular interferometer".[5] Experiments showing the interference of wave packets created by absorption and stimulated emission have been performed on I_2 by Scherer et al.[16] and Na_2 by Baumert et al.[17] The former bears the closest relationship with the process here discussed, in that the interference is controlled by phase locking a sequence of two laser pulses. Both experiments involve oscillating wavepackets in bound potentials, rather than dissociative ones as in our case.

4.C. Rabi Oscillations between Continuum States. The strength of the $1^2\Sigma_u^+ - 2^2\Sigma_g^+$ transition, both in Na_2^+ and in Li_2^+, is a motivation to verify the feasibility of Rabi oscillations between these pairs of states. Notice that both potential curves are repulsive, therefore the probability oscillations would take place between continuum states. Time is here a key variable, because the molecule may dissociate before a complete oscillation has occurred. In fact, to spoil the Rabi oscillations it is sufficient that the wavepackets move to an interval of internuclear distances where the Ω_2 frequency is no more at resonance with the potential energy gap $E(2^2\Sigma_g^+) - E(1^2\Sigma_u^+)$. A semiquantitative theory of the phenomenon[8], based on Rabi's treatment of a two-level system, shows that the final population of the upper state depends on the parameters of the second pulse (τ_2, I_{tot}, I_{max}) as

$$P \approx \sin^2\left(\sqrt{\frac{2\pi I_{tot}\tau_2}{c}}\,\frac{|\mu_{12}|}{\hbar}\right) = \sin^2\left(\sqrt{\frac{2\pi I_{max}}{c}}\,\frac{|\tau_2\mu_{12}|}{\hbar}\right) \quad (8)$$

provided the pulse length τ_2 and the delay t_2 are not too large. If M is the reduced mass, F_1 and F_2 the slopes of the two potential curves, and F their average, the short time requirement is

$$\tau_2^2(\tau_2 + 4t_2) < \frac{8\pi\hbar M}{|F(F_1 - F_2)|} \quad (9)$$

With fast moving wave packets (large t_2F/M) and widely different slopes, the resonance condition changes rapidly in time and very short pulses are needed to observe the Rabi oscillations.

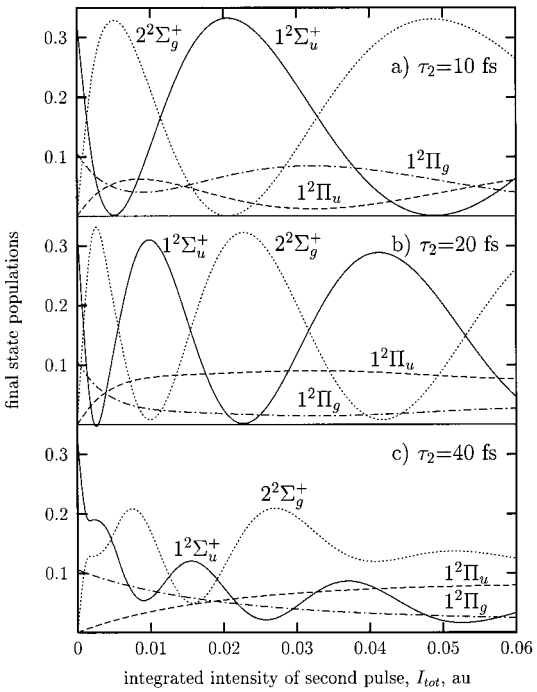

Figure 11. Rabi oscillations of state probabilities in the two-color excitation of Na_2^+, $1^2\Sigma_g^+$, $v = 0$. First pulse: $\tau_1 = 10$ fs, $\Omega_1 = 0.086$ au $= 18875$ cm^{-1}, $I_{tot} = 0.005$ au, $I_{max} = 7.8 \times 10^{10}$ W/cm^2. Second pulse: same as first pulse, but with $\Omega_2 = 0.055$ au $= 12070$ cm^{-1}, and variable intensity.

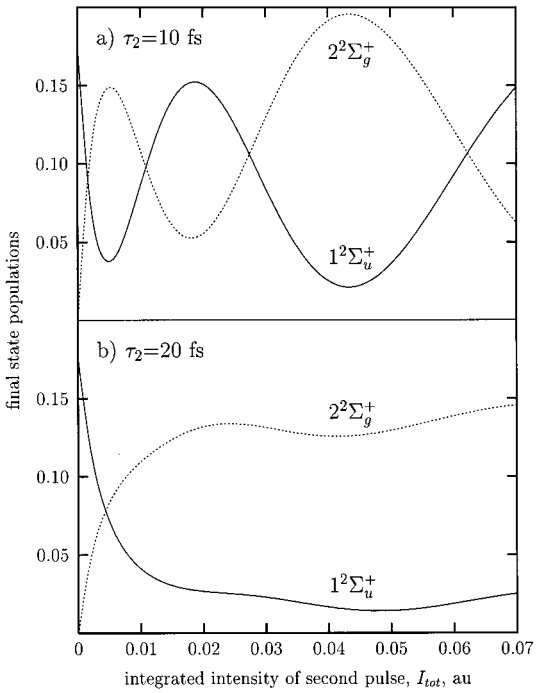

Figure 12. Rabi oscillations of state probabilities in the two-color excitation of Li_2^+, $1^2\Sigma_g^+$, $v = 0$. First pulse: $\tau_1 = 10$ fs, $\Omega_1 = 0.111$ au $= 24140$ cm^{-1}, $I_{tot} = 0.005$ au, $I_{max} = 7.8 \times 10^{10}$ W/cm^2. Second pulse: same as first pulse, but with $\Omega_2 = 0.038$ au $= 8340$ cm^{-1}, and variable intensity.

It is reasonable to envisage experiments where the second laser pulse has a fixed duration and a variable integrated intensity I_{tot}. Simulations on Na_2^+ have shown that the 100% switch of the $1^2\Sigma_u^+$ and $2^2\Sigma_g^+$ populations, seen in Figure 7, corresponds to the first maximum in a plot of the $2^2\Sigma_g^+$ probability versus I_{tot}. With a τ_2 pulse length of 10 or 20 fs a few more minima and maxima can be observed at higher I_{tot} (see Figure 11). The oscillations follow the $\sqrt{I_{tot}\tau_2}$ harmonic law of eq 8. With $\tau_2 =$ 40 fs the oscillations are quite blurred, for the reasons outlined above. In the case of Li_2^+ we find a clear oscillatory behavior with $\tau_2 = 10$ fs but not with $\tau_2 = 20$ fs (see Figure 12). Even with 10 fs the amplitude of the oscillations never reaches 100%. The difference between Na_2^+ and Li_2^+ is due to the smaller reduced mass of the latter, and to the fact that its potential energy curves are steeper and less parallel to each other, all factors which reduce the allowed time for the Rabi phenomenon. It is probable that heavier alkali diatomic ions would be easier testing grounds for this process. Because the radiation-molecular coupling depends on the rotational (*1, m*) quantum numbers, intensity dependent measurements should be performed in the $l = 0$ state.

5. Conclusions

We have studied with realistic computer quantum mechanical simulations the two-photon photodissociation of Na_2^+ and Li_2^+, as compared with the plain one-photon process. A variety of phenomena has been uncovered, all of which can be experimentally observed, at least in principle. As we looked for resonant processes, moderately high laser intensities are needed, of the order of 100 GW/cm^2 for pulse lengths of 10 fs, or proportionally lower peak intensities for longer pulses.

The attention has primarily focussed on above threshold dissociation (ATD), conceived as a bound-free transition followed by a free-free one, with dissociation being a possible outcome of the first as well as of the second excitation step. The photodissociation products of the one- and two-photon processes differ as to their atomic state and kinetic energy content, and their yields depend on the laser frequency in a complementary way. The feasibility of ATD in this scenario depends on the existence of electronic states with suitable potential energy curves and transition dipoles: under this respect, Na_2^+ turns out to be a lucky case, as the comparison with Li_2^+ confirms. However, changing the initial vibrational state or performing two-color experiments introduces a flexibility which makes easier to induce ATD and other multiphoton processes as well.

Two phenomena have drawn our attention: one is the interference between two nonoverlapping laser pulses through the nonstationary dissociating molecular states, which amounts to using the molecule as a microscopic interferometer. The second shows that the concept of Rabi oscillations can be extended to the continuum spectrum, if the laser pulse length is less than the molecular dissociation time.

Although our calculations can be refined, first of all by considering the molecular rotation, and extended to other molecular systems or laser pulse shapes, we are confident that the present results are a sufficient basis to plan at least some of the experiments we propose.

Acknowledgment. This work was supported by grants of the italian MURST. One of the authors (M.P.) thanks the University of Metz for a stage as "professeur invité" in April 1999.

References and Notes

(1) Magnier, S.; Persico, M.; Rahman, N. *Chem. Phys. Lett.* **1997**, *279*, 361.
(2) Magnier, S.; Persico, M.; Rahman, N. *Laser Phys.* **1999**, *9*, 403.
(3) Rahman, N. *J. Phys., Colloq. C1*, Suppl. 1 **1985**, *46*, 249.

(4) Bucksbaum, P. H.; Zavriyev, A.; Muller, H. G.; Schumacher, D. W. *Phys. Rev. Lett.* **1990**, *64*, 1883.

(5) Giusti-Suzor, A.; He, X.; Atabek, O.; Mies, F. H. *Phys. Rev. Lett.* **1990**, *64*, 515.

(6) Jolicard, G.; Atabek, O. *Phys. Rev. A* **1992**, *46*, 5845.

(7) Machholm, M.; Suzor-Weiner, A. *J. Chem. Phys.* **1996**, *105*, 971.

(8) Magnier, S.; Persico, M.; Rahman, N. *Phys. Rev. Lett.* **1999**, *83*, 2159.

(9) Schinke, R. Photodissociation Dynamics; Cambridge University Press: Cambridge, 1993.

(10) Broeckhove, J.; Feyen, B.; Lathouwers, L.; Arickx, F.; Van Leuven, P. *Chem. Phys. Lett.* **1990**, *174*, 504.

(11) Magnier, S.; Masnou-Seeuws, F. *Mol. Phys.* **1996**, *89*, 711.

(12) Magnier, S.; Rousseau, S.; Allouche, A. R.; Hadinger, G.; Aubert-Frécon, M. *Chem. Phys.* **1999**, *246*, 57.

(13) Magnier, S.; Persico, M.; Rahman, N. *Chem. Phys. Lett.* **1996**, *262*, 747.

(14) Labastie, P.; Tribollet, B.; Broyer, M.; Bordas, M. C.; Chevaleyre, J. *Mol. Phys.* **1986**, *59*, 29.

(15) Garraway, B. M.; Stenholm, S. *Phys. Rev.* **1992**, *46*, 1413.

(16) Scherer, N. F.; Carlson, R. J.; Matro, A.; Du, M.; Ruggiero, A. J.; Romero-Rochin, V.; Cina, J. A.; Fleming, G. R.; Rice, S. *A. J. Chem. Phys.* **1991**, *95*, 1487.

(17) Baumert, T.; Engel, V.; Meier, C.; Gerber, G. *Chem. Phys. Lett.* **1992**, *200*, 488.